Alternative Approaches to Magnetic Resonance-Based Electric Properties Tomography and Local Specific Absorption Rate Estimation

**Alternative approaches to magnetic resonance based electric properties tomography and local specific absorption rate estimation**

**Authors**

Alessandro Arduino[a,b]*, Mario Chiampi[a], Luca Zilberti[b], Oriano Bottauscio[b]

**Author affiliation**

[a] Dipartimento Energia – Politecnico di Torino – Corso Duca degli Abruzzi, 24 – 10129 Torino, Italia

[b] Istituto Nazionale di Ricerca Metrologica (INRIM) – Strada delle Cacce, 91 – 10135 Torino, Italia

* Correspondence should be addressed to: alessandro.arduino@polito.it

Published journal article available at DOI: https://doi.org/10.1109/TMAG.2016.2621731

# Alternative Approaches to Magnetic Resonance-based Electric Properties Tomography and Local Specific Absorption Rate Estimation

Alessandro Arduino[1,2], Mario Chiampi[1], Luca Zilberti[2] and Oriano Bottauscio[2], *IEEE Senior Member*

[1]Dipartimento Energia –Politecnico di Torino – Corso Duca degli Abruzzi, 24 – 10129 Torino, Italia
[2]Istituto Nazionale di Ricerca Metrologica (INRIM) – Strada delle Cacce, 91 – 10135 Torino, Italia

**In this paper, three electric properties tomography techniques based on magnetic resonance are applied to a realistic two-dimensional model problem representing the waist of an adult man. The capability of the inverse methods to recover the actual distribution of the electric properties is discussed and compared. In addition, the possibility to extend the methods to the estimate of local specific absorption rate of the radiofrequency field generated in a magnetic resonance imaging, data concerning safety issues, is considered and compared.**

***Index Terms*—electric properties tomography, inverse methods, magnetic resonance imaging, numerical simulation.**

## I. Introduction

THE DOSIMETRIC ISSUES related to the radiofrequency (RF) field generated by the magnetic resonance imaging (MRI) scanners are a relevant topic in safety research [1]-[3]. In particular, one of the physiological effects with respect to safety is tissue heating, which is described in terms of specific absorption rate (SAR) and the relevant standard is IEC 60601-2-33, for the basic safety and essential performance of magnetic resonance equipment for medical diagnosis [4]. To comply with safety issues, numerical techniques and advanced anatomical human models associated with biological tissue properties have been developed in recent years (see for example [5], [6]).

In order to move towards a patient specific dosimetry, quantitative imaging technologies able to determine the electric conductivity and permittivity distribution at RF inside the patient body should be adopted. Nowadays, this kind of technology can be found in microwave imaging [7], [8] that uses a radar system around the inspected body. Clearly, the use of the only MRI scanner should be preferable, in order to limit the introduction of other equipment, possibly more invasive. A first attempt in this direction has been done with the magnetic resonance-based electric impedance tomography [9], [10], that recover the electric properties at low frequencies. In 1991 Haacke and collaborators [11] suggest the possibility to estimate the electric properties at RF starting from the measurement of the RF magnetic field performed by the MRI scanner itself. This method, rediscovered in recent years [12]-[14], has been called the magnetic resonance-based electric properties tomography (denoted by MREPT, or simpler EPT).

A successful implementation of MREPT would lead to additional quantitative information to MRI results useful in many applications other than the safety one [15], [16]. For example, MREPT would help in clinical oncology, because of the higher electric conductivity of some kind of cancerous aggregates with respect to the healthy tissue [17], [18]; and in dosimetry, for example in hyperthermia therapy treatment planning [19], [20].

Probably driven by the prospect of several applications, the scientific community has proposed a plethora of variants for its implementation, which can be divided into at least two main categories of methods: the local and the global ones.

The formers, more similar to the original proposal of Haacke, try to recover the electric properties in each point of the domain by elaborating the electromagnetic (Maxwell's or Helmholtz's) equations locally. These methods have been proved to be feasible in *in vivo* experiments [14], [21], [22]; however strong errors arise at the interfaces between tissues [23] as a consequence of the need of estimating first and second order derivatives of the magnetic field from measured data, often affected by noise. Moreover, the approximation of second order derivatives in presence of sharp variations in electric properties leads to unbounded errors also in ideal noise-free situations. Some techniques have been proposed to fix this kind of errors, like the use of shape-varying kernels [24], [25] or the preliminary recovery of the gradients of the electric properties [26].

On the other hand, global methods study the whole electromagnetic problem at once. Consequently, the recovery of electric properties is performed at a higher computational cost. A first example of global method is reported in [27], where a linear convection-reaction equation is solved using an appropriate numerical method, but, since the coefficients of the proposed partial differential equation are related to the magnetic field derivatives, the difficulty of their estimation still occurs. Some promising methods, recently proposed, deal with the MREPT inverse problem as an optimal control problem [28]-[30], without the need of estimating the magnetic field derivatives.

In this paper, the performances of three main methods are analysed with reference to a noise-free, two-dimensional, model problem. The magnetic field generated at 128 MHz

Manuscript received July 12, 2016. Corresponding author: A. Arduino (e-mail: alessandro.arduino@polito.it).

Color versions of one or more of the figures in this paper are available online at http://ieeexplore.ieee.org.

Digital Object Identifier (inserted by IEEE).

inside a transversal section of the waist of the anatomical human model 'Duke' [31] by a 16-leg birdcage is numerically computed and used as virtual measurement. In order to solve this direct problem, the electric properties of the biological tissues have been taken from the database of IT'IS Foundation [32]. The reconstructed electric properties are compared with the actual properties of the tissues in a statistical framework. Finally, the capability of the methods to estimate the power density dissipated by the electromagnetic radiation in the tissues is evaluated.

## II. Methods

Two local MREPT methods [14], [33] and a global technique [29] are analysed in the following. The local methods have been chosen based on their historical relevance, which is proved by the constant development performed on them [24]-[26], [34] and by their *in vivo* feasibility [14], [21], [22]. Among the global methods, the analysed inverse approach [29], based on the contrast source inversion (CSI) method [35], has been preferred due to the drawbacks of the other techniques. In fact, the direct approach [27] shows the same criticalities of local methods, the approach proposed in [28] is able to recover only the electric conductivity, and technique [30], which deals with a constrained optimization problem, has a more complicated mathematical formulation and would require a higher computational effort.

### A. Local methods

Both the analysed local methods derive from the same partial differential equation for the time-harmonic magnetic field $\boldsymbol{H}$ in isotropic, heterogeneous, magnetically neutral medium:

$$-\nabla^2 \boldsymbol{H} = \frac{1}{\tilde{\varepsilon}} \nabla \tilde{\varepsilon} \times \left( \nabla \times \boldsymbol{H} \right) + \omega^2 \mu_0 \tilde{\varepsilon} \boldsymbol{H} \,. \tag{1}$$

In this equation, written exploiting the phasor notation with reference to the maximum value, $\omega$ is the angular frequency, $\mu_0$ is the magnetic permeability of vacuum and the problem unknown is the complex permittivity of the medium $\tilde{\varepsilon} = \varepsilon_0 \varepsilon_\mathrm{r} - \mathrm{i}\sigma/\omega$ (being $\varepsilon_0$ the vacuum electric permittivity, $\varepsilon_\mathrm{r}$ the relative permittivity and $\sigma$ the equivalent electric conductivity). However, the MRI equipment is able to measure only the rotating component of the magnetic field $H^+$, which rotates in the same wise as the nuclear precession induced by the static field [36] and does not include $H_z$

$$H^+ = \frac{H_x + \mathrm{i} H_y}{2}, \tag{2}$$

where $H_x$ and $H_y$ denote the Cartesian components of the magnetic field transverse to the static field. Thus, the proposed methods restrict the application of (1) to such component, leading to the fundamental equation for the studied local methods:

$$\omega^2 \mu_0 \tilde{\varepsilon} H^+ - \frac{1}{\tilde{\varepsilon}} \left( \frac{\partial \tilde{\varepsilon}}{\partial x} + \mathrm{i} \frac{\partial \tilde{\varepsilon}}{\partial y} \right) \left( \frac{\partial H^+}{\partial x} - \mathrm{i} \frac{\partial H^+}{\partial y} \right) - \frac{1}{\tilde{\varepsilon}} \frac{\partial \tilde{\varepsilon}}{\partial z} \frac{\partial H^+}{\partial z} = -\nabla^2 H^+ . \tag{3}$$

#### 1) Method 1

Method 1 assumes the local homogeneity of the electric properties [14], cancelling the gradients of $\tilde{\varepsilon}$. Consequently, equation (3) reduces to the homogeneous Helmholtz equation for $H^+$, whose inversion leads to the direct formula for the complex permittivity [26]

$$\tilde{\varepsilon} = -\frac{\nabla^2 H^+}{\omega^2 \mu_0 H^+} \,. \tag{4}$$

The simplicity of relation (4) allows an independent reconstruction of relative permittivity and electric conductivity, at the cost of a further approximation for their reconstruction [34]. Precisely, involving only the magnitude of the positively rotating component of the magnetic field $|H^+|$, the relative permittivity can be estimated adopting the formula

$$\varepsilon = -\frac{\nabla^2 \left| H^+ \right|}{\omega^2 \mu_0 \left| H^+ \right|} \,. \tag{5}$$

Conversely, by elaborating only the phase $\varphi^+$ of the magnetic field, the electric conductivity can be estimated as

$$\sigma = \frac{\nabla^2 \varphi^+}{\omega \mu_0} \,. \tag{6}$$

As shown in [14], equation (5) presents the highest errors when $\omega\varepsilon \gg \sigma$, condition verified practically by all the biological tissues at 64 MHz. Vice versa, equation (6) which presents the highest errors when the opposite condition $\sigma \gg \omega\varepsilon$ is verified, is proved to be very useful in the estimate of the electric conductivity of biological tissues [17], [18].

#### 2) Method 2

Method 2 does not introduce approximations in (3), but, to elaborate the equation locally, it assumes in each point of interest the complex permittivity $\tilde{\varepsilon}$ and its derivatives $\left( \partial_x \tilde{\varepsilon} + \mathrm{i} \partial_y \tilde{\varepsilon} \right) / \tilde{\varepsilon}$ and $\left( \partial_z \tilde{\varepsilon} \right) / \tilde{\varepsilon}$ as algebraically independent unknowns [33]. Consequently, a system of at least three linearly independent equations is obtained from (3), where the coefficients are deduced from measurements of magnetic fields generated by linearly independent sources. This task is fulfilled considering linear combinations of the retrieved $H^+$ of individual coil element, which can be measured using multichannel transceiver antennas [33]. The resulting linear system is solved in the least square sense to evaluate the complex permittivity at each node.

It is worth mentioning that the development of this method allows retrieving information on the magnetic field in addition to the measured one when adopting appropriate antennas and sequences [37].

Method 1 and Method 2 require the estimate of the second order derivatives of the rotating magnetic field $H^+$ from the measured data, an operation that is the main source of errors for both methods [23]. In this paper, since the noise in the measured signals is neglected, the inverse operation is simply performed with a second order centred finite difference scheme in the inner nodes, and forward/backward finite differences in the boundary nodes. In presence of noise, some filtering technique like Savitzky-Golay filter [38] can be used to retrieve the information on the derivatives.

Due to the discontinuity of the electric properties, also the Laplacian of the magnetic field is discontinuous at the interfaces between tissues. Thus, errors arise when nodes at the interface between different tissues are included in the kernel of the finite difference scheme. In order to avoid this kind of errors, the derivatives can be computed separately for each material (segmentation), taking advantage in a real application from the result of the imaging procedure. Actually, segmentation is not a trivial task that may merge different tissues into a single region or introduce artificial boundaries, especially when applied to a region with many tissues (as the abdomen). For both local methods, the effect of an ideal segmentation (i.e., able to distinguish precisely each tissue in the domain) as a shape-varying kernel technique is studied.

### *B. Global method*

Method 3 follows a global approach based on Maxwell's equations on the whole region of interest, assuming to know the incident electromagnetic field generated by the RF coil in vacuum [29]. In this paper, where an unshielded birdcage is considered, the scattered electromagnetic field can be exactly formulated in integral form adopting the dyadic Green's functions

$$\mathbf{E}^{\mathrm{s}}[\mathbf{w}](\mathbf{x}) = \int_{\Omega} \mathbf{G}^{\mathrm{EJ}}(\mathbf{x}-\mathbf{y})\mathbf{w}(\mathbf{y})d\mu(\mathbf{y}), \tag{7}$$

$$\mathbf{H}^{\mathrm{s}}[\mathbf{w}](\mathbf{x}) = \int_{\Omega} \mathbf{G}^{\mathrm{HJ}}(\mathbf{x}-\mathbf{y})\mathbf{w}(\mathbf{y})d\mu(\mathbf{y}), \tag{8}$$

with $\mathbf{G}^{\mathrm{EJ}}(\mathbf{r}) = \left(\nabla\nabla + k^2\mathbf{I}\right)\psi(\mathbf{r})$ and $\mathbf{G}^{\mathrm{HJ}}(\mathbf{r}) = \mathrm{i}\omega\varepsilon_0\nabla\psi(\mathbf{r})\times\mathbf{I}$, where $\psi(\mathbf{r})$ is the fundamental solution of the Helmholtz equation with propagation coefficient $k = \omega\sqrt{\varepsilon_0\mu_0}$ and Sommerfeld radiation condition, $\mathbf{I}$ is the identity operator and $\mathbf{w} = \chi\mathbf{E}$ is the contrast source. The contrast function $\chi = \tilde{\varepsilon}/\varepsilon_0 - 1$ is the actual unknown of the MREPT problem. Since the optimization procedure is performed working on the scattered field, the reference data is no longer the positively rotating component of the magnetic field $H^+$ but its scattered portion $H^{+;\mathrm{s}}$.

The objective function of the optimization method is defined as the sum of two contributions: the data cost and the object cost. The former is defined through the data residual, namely the difference between the measured scattered magnetic field and the one produced by the current estimation of the contrast source

$$\rho[\mathbf{w}] = H^{+;\mathrm{s}} - \frac{H_x^s[\mathbf{w}] + \mathrm{i}H_y^s[\mathbf{w}]}{2}. \tag{9}$$

Similarly, the object cost is defined through the object residual, which is the difference between the actual incident contrast source and its current estimation

$$\mathbf{r}[\mathbf{w},\chi] = \chi\mathbf{E}^i - \mathbf{w} + \chi\mathbf{E}^{\mathrm{s}}[\mathbf{w}]. \tag{10}$$

Formally, Method 3 searches the point of minimum $(\mathbf{w}^*, \chi^*)$ of the cost function

$$F[\mathbf{w},\chi] = \frac{\left\|\rho[\mathbf{w}]\right\|^2_{L^2(\Omega)}}{2\left\|H^{+;\mathrm{s}}\right\|^2_{L^2(\Omega)}} + \frac{\left\|\mathbf{r}[\mathbf{w},\chi]\right\|^2_{L^2(\Omega)}}{2\left\|\chi\mathbf{E}^i\right\|^2_{L^2(\Omega)}} \tag{11}$$

The minimization problem is numerically solved adopting a two-step alternating conjugate-gradient update procedure with Polak-Ribière directions [35]. More precisely, by assuming the estimation of the contrast source $\mathbf{w}^{[n-1]}$ and the contrast function $\chi^{[n-1]}$ known at the iterative step *n-1*, at first the contrast source is updated using the conjugate-gradient formula computed with the analytical expression of the gradient of the cost function with respect to the contrast source. Once the new contrast source $\mathbf{w}^{[n]}$ is known, the contrast function is updated solving the minimization problem with respect to it, which reduces to a convex problem whose solution is easily obtained as $\chi^{[n]} = \mathbf{w}^{[n]}\cdot\mathbf{E}^{[n],*} / \mathbf{E}^{[n]}\cdot\mathbf{E}^{[n],*}$, with $\mathbf{E}^{[n]}=\mathbf{E}^i+\mathbf{E}^s[\mathbf{w}^{[n]}]$. The back propagation is used as initial guess for the contrast source [35] and the iterative procedure starts with the contrast function step.

A positivity constraint is imposed on relative permittivity and electric conductivity by simply enforcing unacceptable values of real and imaginary part of the contrast function to zero after each update step [35].

### *C. Estimation of power density*

The local Specific Absorption Rate (SAR) is proportional to the volume density of the power dissipated by the electromagnetic radiation in the tissues, which is quantified by the simple relation

$$p = \sigma\frac{|\mathbf{E}|^2}{2}, \tag{12}$$

where $\mathbf{E}$ is the phasor of the electric field, related to the measurable magnetic field by the Ampère-Maxwell law

$$\mathbf{E} = -\mathrm{i}\frac{1}{\omega\tilde{\varepsilon}}\nabla\times\mathbf{H}. \tag{13}$$

While the complex permittivity (and in particular the electric conductivity) is estimated by any MREPT procedure, the local methods cannot give a direct estimation of the electric field, which is consequently deduced by equation (13). The curl of the magnetic field is approximated neglecting all its components but the positively rotating one, resulting in the relation

$$\nabla\times\mathbf{H} \cong \mathrm{i}\frac{\partial H^+}{\partial z}\hat{\mathbf{i}} + \frac{\partial H^+}{\partial z}\hat{\mathbf{j}} - \left(\mathrm{i}\frac{\partial H^+}{\partial x} + \frac{\partial H^+}{\partial y}\right)\hat{\mathbf{k}}. \tag{14}$$

On the other hand, Method 3 can estimate the electric field by directly applying (7), resulting in a more precise approximation, since no contributions of the magnetic field are neglected. The retrieved electric field is substituted in (12) to evaluate the dissipated power density.

## III. Results and Discussion

The electromagnetic field generated on a section of the waist of the anatomical human model 'Duke' [31] by 16 line sources distributed on a circle of radius 0.356 m has been numerically computed applying a homemade Method of Moments software on a regular grid of 2 mm side. Such source is a two-dimensional approximation of an unshielded birdcage RF antenna working at 128 MHz (corresponding to the Larmor frequency for a 3 T static field). The reference electric properties of the tissues have been taken from the database

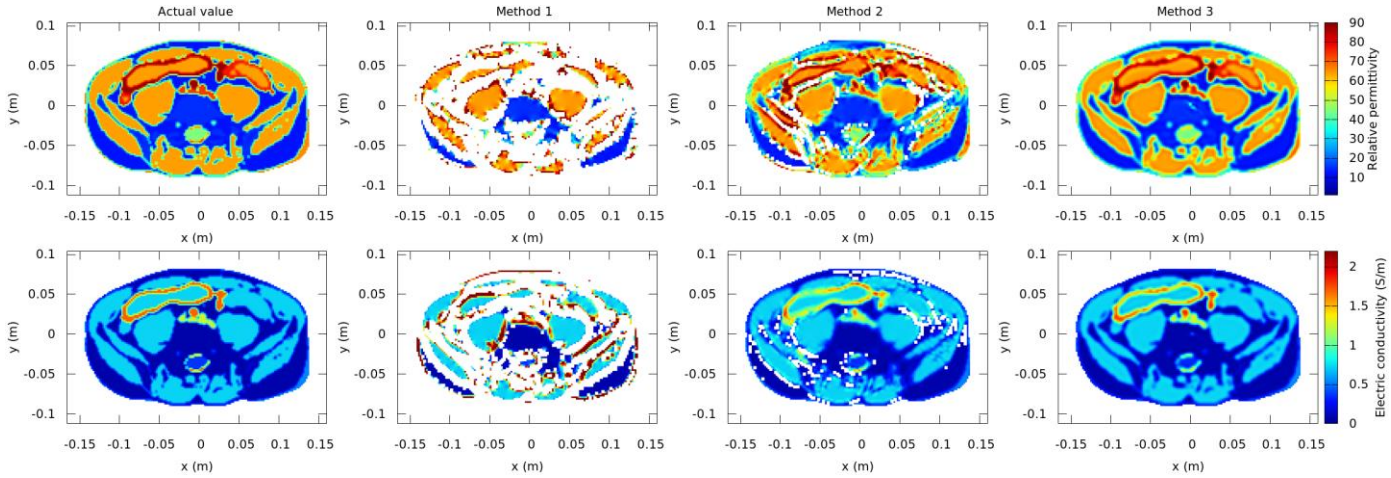


Fig. 1. Section of the waist with the electric tissue properties. First column: actual values; second column: reconstruction with Method 1; third column: reconstruction with Method 2; last column: reconstruction with Method 3 after 1000 iterations. The first row shows the relative permittivity, the second row shows the electric conductivity (S/m). All methods are applied on a 2 mm grid. The values out of range 1-200 for relative permittivity and 0-5 S/m for electric conductivity are discarded.

made available by the IT'IS Foundation [32], which collects data from literature and considers dispersive phenomena. The positively rotating component of the computed magnetic field has been assumed as virtual measurement for the reconstructive methods, using both its magnitude and its phase. In order to obtain more than one linearly independent magnetic field value for Method 2, the sources are collected in groups of four lines disposed symmetrically on the circle and only one group was switched-on at each simulation. Nonetheless, a comparison with an asymmetric distribution of the sources is performed considering groups of four consecutive lines, each one driven with the same current magnitude but a different phase, corresponding to the angular position of the line itself. Such configuration is clearly unphysical, since the summation of the currents crossing the 2D domain is different from zero, but it is useful for a theoretical demonstration, anyway. In the following, unless otherwise stated, Method 2 has to be considered applied to the former configuration. When needed, the field generated by the sources in vacuum has been directly computed applying the convolution integrals with the dyadic Green's functions.

The reference electric properties of the studied domain are reported in the first column of Fig. 1, which collects also the reconstructions achieved by the three methods on a regular grid of 2 mm, showing both the relative permittivity (top) and the electric conductivity (bottom). When the reconstructive technique led to a negative or too high value (over 200 for relative permittivity and over 5 S/m for electric conductivity) in a point, that value has been discarded. The considered region presents many tissues, some of them spatially very confined in at least one direction. Thus, the hypothesis of local homogeneity of Method 1 is often not fulfilled and in many points the reconstructed value is discarded (Fig. 1, column 2). Method 2 reaches better results since no hypotheses are introduced in its formulation; nonetheless, almost the totality of its errors are located at interfaces between tissues, confirming the criticality of Laplacian estimation (Fig. 1, column 3). Finally, Method 3 after 1000 iterations shows a further reduced

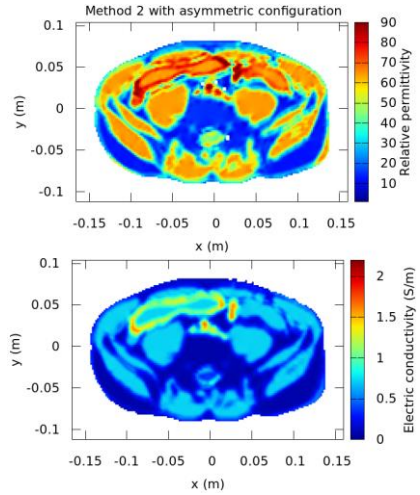


Fig. 2. Reconstruction of relative permittivity and electric conductivity with Method 2 applied to asymmetric configuration. As for Fig. 1, the method is applied on a 2 mm grid, and the values out of range 1-200 for relative permittivity and 0-5 S/m for electric conductivity are discarded.

error, since no reconstructed value has been discarded and very small details, like blood vessels and cerebrospinal fluid, are accurately recovered (Fig. 1, column 4). The higher accuracy comes together with a higher computational demand: on a standard desktop PC, our homemade sequential C++ code requires about 7 minutes to perform 1000 iterations of Method 3, 1.2 s for the execution of Method 2 and 0.05 s for Method 1. Method 3 has been applied with 1000 iterations because at this point the root mean square error almost reaches its minimum. Nonetheless, the following considerations would remain the same if using only 300 iterations, which require about 2 minutes of computations. It is also important to underline that some margin of optimization is still possible (e.g., by parallelizing the code); thus, a prospective of improvement from the computational point of view can be envisaged.

The reconstructions achieved by Method 2 when applied to the asymmetric groups of sources are reported in Fig. 2. It is evident a sensible reduction of discarded points with respect to

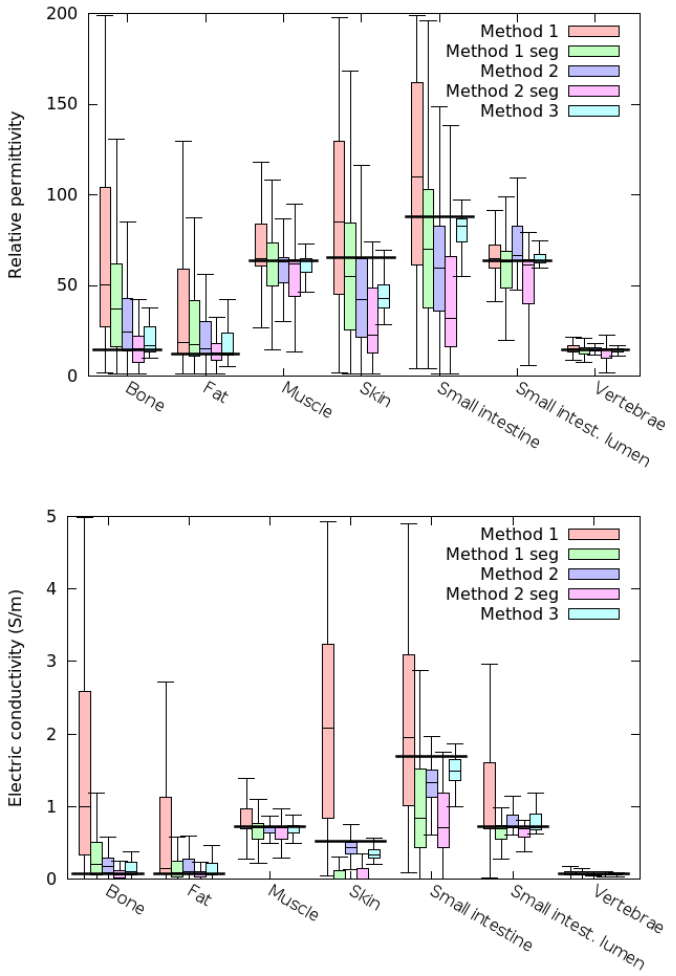


Fig. 3. Boxplot divided into quartiles of the estimated electric properties in the more extended tissues. The black horizontal line is the actual value. Method 3 is stopped after 1000 iterations. Values out of range 1-200 for relative permittivity and 0-5 S/m for electric conductivity are outliers.

the previous application of Method 2 (almost all the pixels are reconstructed) and the compensation of the error in Laplacian estimation at the interfaces, which in this case are smoothly recovered. This improvement has a twofold explanation. On one side, the asymmetric groups generate magnetic fields that are more different one to each other than those generated by the regular groups, especially in the central region; thus, more information are elaborated in the linear system behind Method 2. On the other side, since the magnetic fields generated by the asymmetric groups are more heterogeneous than the other ones, the derivatives can be approximated more precisely.

More quantitative considerations can be developed referring to Fig. 3, where the boxplots of the estimated electric properties, divided into quartiles, are collected for the most extended tissues, whose distribution in the domain is mapped in Fig. 4. The behaviour of the tissues taken into account is very different, due to their various geometrical distributions. For this reason the distinction between bone and vertebrae is convenient, despite the two are actually made of the same material. Looking at Fig. 3, it results that both bone and fat show a similar statistical distribution of the reconstruction, coherently with the

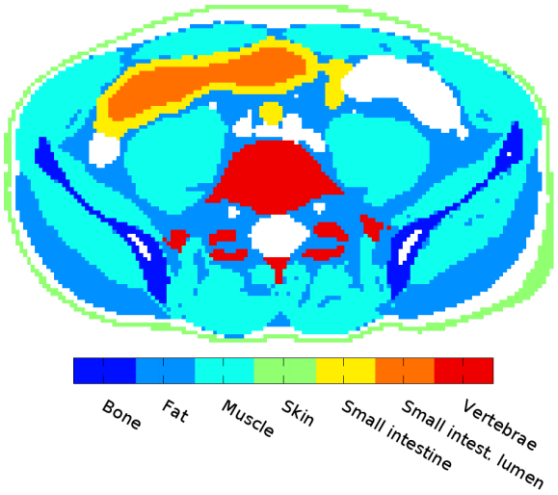


Fig. 4. Map of the largest tissues in the investigated section.

fact that their electric properties are quite similar and that both possess very narrow or isolated regions surrounded by tissues with quite different electric properties (predominantly muscle). The introduction of segmentation in both Method 1 and Method 2 reduces the variance in bone and fat estimation. It also increases the percentage of admissible point reconstructions in Method 1 (Table 1), but, on the other hand, it decreases the one of Method 2, since many segmented points are too isolated to allow the derivative computation on them. Although the electric properties of vertebrae are the same of bones, their reconstruction is much better than the ones of both the previously considered tissues. This is because vertebrae are surrounded by fat, which has very similar electric properties, and so the derivatives (included the Laplacian) are well estimated in every point of the domain. Since some points are too isolated for the derivatives approximation, the introduction of segmentation slightly worsens the reconstruction.

Since bone, fat and vertebrae have similar electric properties, they can be grouped and assumed to be segmented in a single region. The result of this segmentation, not reported in tables or figures, is interesting. By reducing the imposed interfaces, the number of reconstructed pixels increases for both Method 1 and 2. Precisely, the number of recovered pixels in the group passes from 62.7 % to 66.56 % for relative permittivity and from 62.3 % to 65.0 % for electric conductivity in case of Method 1, whereas for Method 2 it moves from 75.3 % to 80.2 % and from 78.3 % to 83.7 % for relative permittivity and electric conductivity, respectively. However, in the case of Method 2 the absence of segmentation is still favourable. In addition, the variance of the reconstruction of the group increases for Method 1 (+2.7 % for relative permittivity and +11.0 % for electric conductivity) and for the reconstruction of electric conductivity with Method 2 (+1.5 %), but slightly decreases for Method 2 relative permittivity reconstruction (-3.8 %).

The muscle is the widest tissue in the studied region, constituted by many sub-regions of grouped pixels. The percentage of reconstruction (Table 1) is high for all methods; in particular, Method 1 shows a little advantage when performed using the segmentation, although the variance of the

TABLE I
PERCENTAGE OF RECONSTRUCTED PIXELS

| | Extension in pixels | Method 1 | | Method 1 seg | | Method 2 | | Method 2 seg | | Method 3 | |
|---|---|---|---|---|---|---|---|---|---|---|---|
| | | $\varepsilon_r$ | $\sigma$ | $\varepsilon_r$ | $\sigma$ | $\varepsilon_r$ | $\sigma$ | $\varepsilon_r$ | $\sigma$ | $\varepsilon_r$ | $\sigma$ |
| Bone | 383 | 39.1 % | 43.8 % | 53.0 % | 57.7 % | 86.1 % | 89.5 % | 68.4 % | 72.5 % | 100 % | 100 % |
| Fat | 2612 | 52.4 % | 58.9 % | 59.5 % | 56.8 % | 92.7 % | 93.5 % | 72.9 % | 76.4 % | 100 % | 100 % |
| Muscle | 4027 | 65.3 % | 70.1 % | 83.7 % | 85.7 % | 97.0 % | 99.5 % | 94.4 % | 97.2 % | 100 % | 100 % |
| Skin | 553 | 42.4 % | 30.1 % | 23.6 % | 26.9 % | 85.3 % | 100 % | 29.2 % | 36.5 % | 100 % | 100 % |
| Small intestine | 414 | 21.4 % | 44.6 % | 54.8 % | 78.7 % | 90.5 % | 100 % | 71.4 % | 98.0 % | 100 % | 100 % |
| Small intestine lumen | 400 | 64.5 % | 74.5 % | 84.7 % | 95.0 % | 100 % | 100 % | 94.0 % | 100 % | 100 % | 100 % |
| Vertebrae | 602 | 87.5 % | 88.7 % | 82.5 % | 89.0 % | 98.6 % | 98.5 % | 90.1 % | 90.1 % | 100 % | 100 % |

For each method, the percentage of punctual values reconstructed in the range 1-200 for relative permittivity ($\varepsilon_r$) and 0-5 S/m for electric conductivity ($\sigma$) are collected for the most extended tissues (the extension in square pixels with 2 mm side is reported). Method 3 is stopped after 1000 iterations.

recovered values (Fig. 3) does not change. On the other hand, the segmentation increases the variance in muscle reconstruction using Method 2, and reduces its percentage of reconstruction. Method 3, which recovers acceptable values in any point of the domain (Table 1), has the best variance for muscle relative permittivity estimation, whereas it is equivalent to Method 2 looking for the electric conductivity.

Both the skin and the small intestine are thin tissues. Thus, although their electric properties are very different, the qualitative behaviour of their reconstruction is the same. Method 1 is unable to reconstruct them: only a few points are recovered and with a very high variance. There is no benefit in the application of the segmentation for these tissues, since many points are discarded being too isolated for derivatives approximation, and the remaining points show a wide variance for relative permittivity and almost all have null electric conductivity. Both Method 2 and Method 3 underestimate the properties of thin tissues. Method 3 guarantees a smaller variance near the actual values, anyway.

Finally, the small intestine lumen is a wide compact region with quite different electric properties with respect to the surrounding wall (i.e., the small intestine) and all methods recover it relatively well. The segmentation worsens the relative permittivity estimation, whereas sensibly improves the one of electric conductivity, by increasing the number of acceptable values and decreasing their variance.

As previously observed for bone, fat and vertebrae, also muscle, skin and small intestine lumen are tissues with very similar electric properties. However, to group them in a single region during segmentation does not change the reconstruction, since these tissues are separated and the number of imposed interfaces would remain the same.

The estimation of the power density dissipated by the RF electromagnetic radiation in the tissues is a complex task, also taking into account that Method 1 and Method 2 provide negative values of the electric properties in some points of the domain. By noticing that the actual value of each tissue is often close to the mean value recovered for it (Fig. 3), the issue may be overcome adopting, for each tissue, the corresponding mean value. Since such approach requires the segmentation of the domain (needed to distinguish to which tissue each point belongs), Method 1 and Method 2 have been applied using the shape-varying kernel regularization in order to reduce the variances and improve the quality of the mean (Fig. 3). Since Method 3 recovers no points with unreasonable values, the power density estimation has been performed directly on its

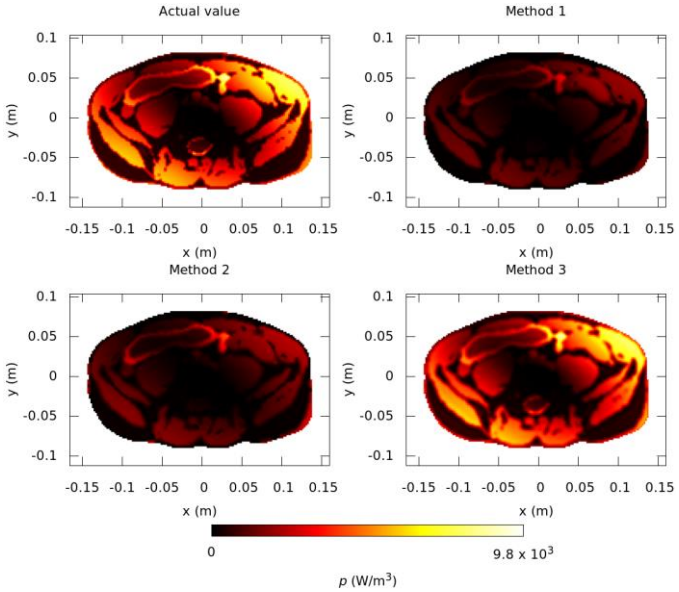


Fig. 5. Section of the waist with the power density dissipated by the electromagnetic radiation in the worst-case scenario, namely the whole body SAR (computed on the slice) is equal to 2 W/Kg. From left to right, in the first row are reported the reference values, and the reconstruction with Method 1 using segmentation; in the second row the reconstruction with Method 2 using segmentation, and the reconstruction with Method 3 after 1000 iterations. All methods are applied on a 2 mm grid.

reconstruction of the electric properties. The actual value and the estimations of the dissipated power density are reported in Fig. 5 in the worst-case scenario, namely in case of an actual average SAR evaluated on the slice equal to 2 W/kg. For SAR computation the densities of the tissues collected in [32] are adopted. As can be deduced by analysing Fig. 5, all methods are able to identify the hotspots location, but only Method 3 is quantitatively precise regarding the intensity. This is due to the fact that Method 3, by recovering the whole scattered electromagnetic field together with the electric properties, implicitly considers the effects of the components of the magnetic field that is not rotating in the nuclei precession wise, that are neglected in the relation (14).

## IV. CONCLUSION

In this paper, three main approaches for the MR-based EPT have been compared, focusing on their capability to recover the electric properties properly, as well as to estimate the power density dissipated by the RF radiation in the patient during the examination. In order to study the methods in an equivalent context, they have been applied to a virtual two-dimensional

model problem where the electromagnetic field generated by a 128 MHz birdcage on a transverse section of a human waist model has been numerically computed and used as virtual measurement. In addition, in order to focus on modelling and numerical errors, noise-free measurements have been used, namely an infinite signal to noise ratio (SNR) in the signal acquired by the MRI scanner has been assumed. Clearly, noise propagation through the methods and effects of different filtering techniques require further specific studies, as the one performed in [39] for Method 1.

The analysis of the recovered electric properties suggests that Method 3 leads to the best results in terms of accuracy, but at the cost of a higher computational demand with respect to the other methods. In particular, Method 2, without the adoption of segmentation based regularization techniques, recovers the electric properties a little worse than Method 3 but much faster. Consequently, in order to use global techniques for real-time applications (e.g., in clinics) more technological advances in software implementation are required (cluster parallelization, hardware acceleration), whereas at the state of the art it appears easier to rely on local methods when a rough image of electric properties distribution is required.

The interpretation of the results change when one refers to applications where processing time is less crucial and/or a more precise reconstruction is required, as for example in the hyperthermia treatment planning, or where information that are not accessible using local methods are required, like in MRI safety. Having in mind this last particular application, the possibility to estimate the dissipated power density as an extension of the MREPT methods has been studied. The results suggest that the contribution to the electric field due to the components of the magnetic field that are not rotating in the nuclei precession wise, neglected in the relation (14) used by local methods but implicitly considered by Method 3, may play a crucial role in the energy deposition on the patient. The neglected components are expected to be significant, for example, in case of ultra high field (UHF) MRI or when surface coils are used. Thus, although local methods prove to be able to localize the hotspots, they cannot quantitatively estimate them.

Clearly, the achieved results are not completely general, because obtained by analysing only one particular section of the abdominal region. Some considerations may change when a different slice is studied or a different orientation is considered (e.g., a coronal slice). When an efficient three-dimensional implementation of Method 3, which up to now has not been described in literature yet, will be available, it would be interesting to reproduce this analysis in three dimensions, with the aim of taking into account all the possible complex interactions among different tissues.

However, this work suggests with no doubt the importance of further studies on global methods, and in particular on Method 3, for safety applications, where the local dissipated power density is a requirement. At least two contributions on the progress of global methods can be distinguished: the development of more advanced software in order to reduce the time of execution of the procedures and guarantee their applicability in three dimensions, and the study of their feasibility *in vivo*.

## REFERENCES


[1] S. Sammet, "Magnetic resonance safety", *Abdom. Radiol.*, vol. 41, pp. 444–451, 2016.

[2] S. M. Park, R. Kamondetdacha, A. Amjad and J. A. Nyenhuis, "MRI safety: RF-induced heating near straight wires," *IEEE Trans. Magn.*, vol. 41, pp. 4197-9, Oct. 2005.

[3] M. Lu and S. Ueno, "Dosimetry of exposure of patients to pulsed gradient magnetic fields in MRI," *IEEE Trans. Magn*., vol. 47, no. 10, pp. 1841–1844, Oct. 2011

[4] International Electrotechnical Commission 2010 Medical electrical equipment - Part 2-33: Particular requirements for the basic safety and essential performance of magnetic resonance equipment for medical diagnosis IEC 60601-2-33 Ed. 3.

[5] M. Gosselin et al., "Development of a new generation of high-resolution anatomical models for medical device evaluation: the Virtual Population 3.0", *Phys. Med. Biol*., vol. 59, n. 18, pp. 5287-5303, Sept. 2014.

[6] O. Bottauscio, M. Chiampi, J. Hand and L. Zilberti, "A GPU computational code for eddy-current problems in voxel-based anatomy," *IEEE Trans. Magn.*, vol. 51, Mar. 2015.

[7] L. Yang, S. L. Ho, S. Yang and W. Fu, "Numerical analysis of inverse scattering in microwave imaging," *IEEE Trans. Magn.*, vol. 47, pp. 1482-5, May 2011.

[8] L. Yang, S. Yang, S. L. Ho and W. N. Fu, "An improved evolution strategy and its application to inverse scattering in microwave imaging," *IEEE Trans. Magn.*, vol. 51, Mar. 2015.

[9] J. K. Seo and E. J. Woo, "Electrical tissue property imaging at low frequency using MREIT," *IEEE Trans. Med. Imag.*, vol. 61, pp. 1390-9, May 2014.

[10] N. De Geeter, G. Crevecoeur and L. Dupré, "A numerical study on conductivity estimation of the human head in the low frequency domain using induced current MR phase imaging EIT with multiple gradients," *IEEE Trans. Magn.*, vol. 49, pp. 5004-10, Sept. 2013.

[11] E.M. Haacke, L.S. Petropoulos, E.W. Nilges and D.H. Wu, "Extraction of conductivity and permittivity using magnetic resonance imaging," *Phys. Med. Biol.*, vol. 36, pp. 723-34, June 1991.

[12] U. Katscher et al., "Determination of Electric Conductivity and Local SAR Via B1 Mapping," *IEEE Trans. Med. Imag*., vol. 28, pp. 1365-74, Sept. 2009.

[13] U. Katscher, T. Voigt and C. Findeklee, "Electrical conductivity imaging using magnetic resonance tomography," *Conf. Proc. IEEE Eng. Med. Biol. Soc.*, Minneapolis, Minnesota, USA, 2009, pp. 3162-3164.

[14] T. Voigt, U. Katscher and O. Doessel, "Quantitative Conductivity and Permittivity Imaging of the Human Brain Using Electric Properties Tomography," *Magn. Reson. Med.*, vol. 66, pp. 456-66, Aug. 2011.

[15] T. Voigt, H. Homann, U. Katscher and O. Doessel, "Patient-individual local SAR determination: in vivo measurements and numerical validation," *Magn. Reson. Med.*, vol. 68, pp. 1117-26, Oct. 2012.

[16] X. Zhang et al., "Quantitative prediction of radio frequency induced local heating derived from measured magnetic field maps in magnetic resonance imaging: a phantom validation at 7T," *Appl. Phys. Lett.*, vol. 105, pp. 244101, Dec. 2014.

[17] J. Shin et al., "Initial study on in vivo conductivity mapping of breast cancer using MRI," *J. Magn. Reson. Imag*., vol. 42, pp. 371-8, Aug. 2015.

[18] E. Balidemaj et al., "Feasibility of electric property tomography of pelvic tumors at 3T," *Magn. Reson. Med.*, vol. 73, pp. 1505-13, Dec. 2015.

[19] C. A. T. Van den Berg et al., "MR and hyperthermia: exploiting similarities for mutual benefit," in *Proc. 42nd Eur. Microw. Conf.*, Amsterdam, The Netherlands, 2012, pp. 632-635.

[20] H. P. Kok et al., "Current state of the art of regional hyperthermia treatment planning: a review," *Radiat. Oncol.*, vol. 10, pp.196, Sept. 2015.

[21] A.L. Van Lier et al., "B1+ Phase Mapping at 7 T and its Application for In Vivo Electrical Conductivity Mapping," *Magn. Reson. Med.*, vol. 67, pp. 552-61, Feb. 2012.

[22] X. Zhang, P.F. Van de Moortele, S. Schmitter and B. He, "Complex B1 Mapping and Electrical Properties Imaging of the Human Brain Using a 16-channel Transceiver Coil at 7 T," *Magn. Reson. Med.*, vol. 69, pp. 1285-96, May 2013.

[23] J.K. Seo et al., "Error Analysis of Nonconstant Admittivity for MR-Based Electric Property Imaging," *IEEE Trans. Med. Imag.*, vol. 31, pp. 430-7, Feb. 2012.

[24] U. Katscher et al., "Estimation of Breast Tumor Conductivity Using Parabolic Phase Fitting," in *Proc. 20th Annual Meeting of ISMRM*, Melbourne, Australia, 2012, pp. 2335.
[25] L. Huang et al., "A Monte Carlo Method for Overcoming the Edge Artifacts in MRI-based Electrical Conductivity Mapping," in *Proc. 22th Annual Meeting of ISMRM*, Milan, Italy, 2014, pp. 3190.
[26] J. Liu et al., "Gradient-Based Electrical Properties Tomography (gEPT): A Robust Method for Mapping Electrical Properties of Biological Tissues In Vivo Using Magnetic Resonance Imaging," *Magn. Reson. Med.*, vol. 74, pp. 634-46, Sept. 2015.
[27] F.S. Hafalir, O.F. Oran, N. Gurler and Y.Z. Ider, "Convection-Reaction Equation Based Magnetic Resonance Electrical Properties Tomography (cr-MREPT)," *IEEE Trans. Med. Imag.*, vol. 33, pp. 777-93, March 2014.
[28] A. Borsic, I. Perreard and R.J. Halter, "An Inverse Approach to MR-EPT Reconstruction," in *Proc. 22th Annual Meeting of ISMRM*, Milan, Italy, 2014, pp. 3191.
[29] E. Balidemaj et al., "CSI-EPT: A Constrast Source Inversion Approach for Improved MRI-Based Electric Properties Tomography," *IEEE Trans. Med. Imag.*, vol. 34, pp. 1788-96, Sept. 2015.
[30] H. Ammari et al., "Magnetic resonance-based reconstruction method of conductivity and permittivity distributions at the Larmor frequency," *Inverse Problems*, vol. 31, pp. 105001, Oct. 2015.
[31] A. Christ et al. "The Virtual Family - Development of Surface-based Anatomical Models of Two Adults and Two Children for Dosimetric Simulations," *Phys. Med. Biol.*, vol. 55, pp. N23-38, Jan. 2010.
[32] IT'IS Foundation (2016). Database for thermal and electromagnetic parameters of biological tissues. [Online]. Available: http://www.itis.ethz.ch/database
[33] X. Zhang et al., "From Complex B1 Mapping to Local SAR Estimation for Human Brain MR Imaging Using Multi-Channel Transceiver Coil at 7T," *IEEE Trans. Med. Imag.*, vol. 32, pp. 1058-67, June 2013.
[34] U. Katscher, D.H. Kim and J.K. Seo, "Recent Progress and Future Challenges in MR Electric Properties Tomography," *Comput. Math. Method M.*, pp. 546-62, 2013.
[35] P.M. Van den Berg and A. Abubakar, "Constrast Source Inversion Method: State of the Art," *Prog. Electromagn. Res.*, vol. 34, pp. 189-218, 2001.
[36] D.I. Hoult "The Principle of Reciprocity in Signal Strength Calculations - A Mathematical Guide," *Concepts Magn. Reson.*, vol. 12, n. 4, pp. 173-87, 2000.
[37] X. Zhang, J. Liu and B. He, "Magnetic-Resonance-Based Electrical Properties Tomography: A Review," *IEEE Rev. Biomed. Eng.*, vol. 7, pp. 87-96, 2014.
[38] A. Savitzky, M.J.E. Golay, "Smoothing and differentiation of data by simplified least squares procedures," *Anal. Chem.*, vol. 36, pp. 1627-39, July 1964.
[39] S.K. Lee, S. Bulumulla and I. Hancu, "Theoretical investigation of random noise-limited signal-to-noise ratio in MR-based electrical properties tomography," *IEEE Trans. Med. Imag.*, vol. 34, pp. 2220-32, Nov. 2015.